

Deuterium and Oxygen Toward Feige 110: Results from the Far Ultraviolet Spectroscopic Explorer (*FUSE*) Mission

S.D. Friedman¹, J.C. Howk¹, P. Chayer^{1,2}, T.M. Tripp³, G. Hébrard⁴, M. André¹, C. Oliveira¹, E.B. Jenkins³, H.W. Moos¹, W.R. Oegerle⁵, G. Sonneborn⁵, R. Lamontagne⁶, K.R. Sembach¹, A. Vidal-Madjar⁴

ABSTRACT

We present measurements of the column densities of interstellar D I and O I made with the *Far Ultraviolet Spectroscopic Explorer (FUSE)*, and of H I made with the *International Ultraviolet Explorer (IUE)* toward the sdOB star Feige 110 $[(l,b) = (74^{\circ}09, -59^{\circ}07); d = 179_{-67}^{+265}$ pc; $z = -154_{-227}^{+57}$ pc]. Our determination of the D I column density made use of curve of growth fitting and profile fitting analyses, while our O I column density determination used only curve of growth techniques. The H I column density was estimated by fitting the damping wings of the interstellar Ly α profile. We find $\log N(\text{D I}) = 15.47 \pm 0.06$, $\log N(\text{O I}) = 16.73 \pm 0.10$, and $\log N(\text{H I}) = 20.14_{-0.20}^{+0.13}$ (all errors 2σ). This implies $\text{D}/\text{H} = (2.14 \pm 0.82) \times 10^{-5}$, $\text{D}/\text{O} = (5.50_{-1.33}^{+1.64}) \times 10^{-2}$, and $\text{O}/\text{H} = (3.89 \pm 1.67) \times 10^{-4}$. Taken with the *FUSE* results reported in companion papers (Moos et al. 2001) and previous measurements of the local interstellar medium, this suggests the possibility of spatial variability in D/H for sight lines exceeding ~ 100 pc. This result may constrain models which characterize the mixing time and length scales of material in the local interstellar medium.

Subject headings: Cosmology: Observations – ISM: abundances – Ultraviolet: ISM – stars: Individual (Feige 110)

1. Introduction

Precise measurements of primordial abundances of the light elements deuterium (D), ³He, ⁴He, and ⁷Li relative to hydrogen have been a goal of astronomers for many years. In the standard Big Bang nucleosynthesis model, these quantities are related in a straightforward way to the baryon-to-photon ratio in the early universe, from which Ω_{B} , the fraction of the critical density contributed by baryons, may be determined (Boesgard & Steigman 1985). In principle, a measurement of any single one of these abundance ratios would be sufficient to determine Ω_{B} . In practice, however, the D/H ratio is more useful than the others for two reasons: (1) D/H is a stronger function of Ω_{B} than the other light element ratios, and will yield a more accurate value of Ω_{B} . (2) The only appreciable source of deuterium is the Big Bang itself. No other significant production mechanisms have been identified (Reeves et al. 1973; Epstein, Lattimer, & Schramm 1976).

¹Department of Physics & Astronomy, The Johns Hopkins University, Baltimore, MD 21218; scott@pha.jhu.edu

²Department of Physics & Astronomy, University of Victoria, P.O. Box 3055, Victoria, BC V8W 3P6, Canada

³Princeton University Observatory, Princeton, NJ 08544

⁴Institut d'Astrophysique de Paris, CNRS, 98 bis bld Arago, F-75014 Paris, France

⁵Laboratory for Astronomy and Solar Physics, NASA/GSFC, Code 681, Greenbelt, MD 20771

⁶Univ. de Montréal, Dept. de Physique, CP 6128 Succ. Centre-Ville, Montréal, PQ H3C 3J7 Canada

Since deuterium is easily destroyed in stellar interiors, the D/H ratio is expected to monotonically decrease with time. This makes the interpretation of a D/H measurement simpler than the corresponding ratios for the other species.

Measurements of D/H in the local interstellar medium (ISM), as the present work reports, have been made using *Copernicus* (Rogerson & York 1973; see also the review by Vidal-Madjar & Gry 1984), *HST* (e.g., Linsky et al. 1995; Vidal-Madjar et al. 1998; Sahu et al. 1999), *ORFEUS* (Gözl et al. 1998; Bluhm et al. 1999), and *IMAPS* (Jenkins et al. 1999; Sonneborn et al. 2000). These local ISM measurements represent a lower limit to the primordial value. When corrected for the effects of astration (Tosi et al. 1998), the results should be comparable to those obtained in low-metallicity, high redshift Ly α clouds (Kirkman et al. 2000; Burles & Tytler 1998), which should be very nearly the primordial value itself.

In this paper we present the results of an analysis of the sight line toward Feige 110, an sdOB star located at a distance of 179_{-67}^{+265} pc. We derive D I and O I column densities with data obtained from the *Far Ultraviolet Spectroscopic Explorer (FUSE)*, and estimate the H I column density with data from the *International Ultraviolet Explorer (IUE)*. This is the most distant target of the initial set of *FUSE* studies (Hébrard et al. 2001; Kruk et al. 2001; Lehner et al. 2001; Lemoine et al. 2001; Sonneborn et al. 2001; Wood et al. 2001) of deuterium in the local interstellar medium. The results of these studies are summarized by Moos et al. (2001), who discuss the general nature and importance of the D/H problem, the implications of the results in the context of previous D/H measurements, and how they relate to other observational results, such the spatial variability of O/H and N/H in the interstellar medium.

In §2 we present a summary of the observations and a description of the data reduction processes. In §3 the stellar model of Feige 110 is discussed, as well as properties of the sight line and distance estimates to the star. The details of the analysis of the D I and O I column densities are given in §4, and the H I analysis is presented in §5. In §6 we discuss the results of this study.

2. Observations and Data Processing

The *FUSE* instrument has a bandpass of 905-1187 Å. It consists of four co-aligned telescopes illuminating separate Rowland-circle spectrograph channels. Each channel is comprised of a diffraction grating and a portion of a detector. Each of the two large-area, two-dimensional detectors has two microchannel-plate segments, designated A and B, which are coated with KBr photocathodes. The detectors record the position of each incident photon. The telescope mirrors and gratings of two channels are coated with SiC, and those of the remaining two channels are coated with LiF over aluminum. Detector 1 records the light from the SiC1 and LiF1 channels, and detector 2 from the SiC2 and LiF2 channels. The dispersion of the SiC and LiF channels is 6.2 and 6.7 mÅ pixel⁻¹, respectively. The *FUSE* resolution is approximately 15 - 20 km s⁻¹ (FWHM). A detailed description of the *FUSE* mission is given by Moos et al. (2000), and the instrumentation and performance is described by Sahnou et al. (2000).

Feige 110 was observed with *FUSE* for a total of 28 ksec under two separate programs, M1080801 and P1044301. The observation log is shown in Table 1. All data were obtained in histogram mode using the LWRS (30'' × 30'') aperture.

The data were reduced using CALFUSE pipeline version 1.8.7. The individual 1-dimensional spectra were co-added to form the final spectrum for each channel and detector segment separately after removing the relative shifts between individual spectra on the detector caused by image and grating motion (Sahnou et

al. 2000). The shifts were determined by cross-correlating the individual spectra over a limited wavelength range which contained prominent spectral features but no airglow lines. Typical shifts were $\lesssim 4$ pixels, or $\lesssim 0.025\text{\AA}$. Although *FUSE* observations of H I and O I lines are sometimes contaminated by airglow emission, requiring the use of data obtained only during spacecraft orbital night, it was found that this was unimportant in our analysis, and the combined day and night data were used.

Most of our analysis was based on SiC1B and SiC2A spectra ($910 \lesssim \lambda \lesssim 1005 \text{\AA}$), which span the high order Lyman lines (Ly γ through the Lyman limit). SiC2A generally has somewhat better spectral resolving power, but also suffers from more detector fixed-pattern noise. In rare cases, fixed-pattern features can cause the detector response to vary by as much as 20% over very small scales, and while the resulting spectral features are sometimes diminished by the motion of the spectra on the detectors (Sahnou et al. 2000) they are not explicitly removed in the current CALFUSE pipeline reduction. This difficulty is ameliorated by the multiple channel design of *FUSE*; measurements of absorption lines that appear in the spectra of more than one channel are independent, which can help to distinguish between real and instrumentally-induced spectral features.

Figure 1 shows the co-added SiC2A spectrum of Feige 110, which covers the wavelength range 916 - 1007 \AA . D I, O I, and other lines arising in the ISM are identified. The spectral resolution is about 17 km s $^{-1}$ (FWHM). Typical S/N ratios for this observation are between 20 and 25.

The H I column density along this line of sight was estimated using the Lyman α profile from the single high resolution spectrum of Feige 110 taken with *IUE*. The 15.3 ksec observation was made on 15 October 1981 (see Table 1), and reduced using IUESIPS. The analysis of these data is discussed in more detail in §5.

3. The Line of Sight to and Stellar Spectrum of Feige 110

Table 2 summarizes the important properties of Feige 110 and the sight line to this star. The trigonometric parallax of Feige 110 was measured to be $\pi = 5.59 \pm 3.34$ milliarcsec using the Hipparcos satellite (Perryman et al. 1997), which yields a distance of 179_{-67}^{+265} pc. The star lies in the direction $(l,b) = (74^\circ 09', -59^\circ 07')$ at $z = -154_{-227}^{+57}$ pc from the Galactic plane, well beyond the local interstellar cloud (Lallement & Bertin 1992), and probably beyond most of the neutral hydrogen associated with the wall of the Local Bubble (Sfeir et al. 1999). This is not true of most of the other local ISM sight lines studied with *FUSE* (see Moos et al. 2001 and references therein). Therefore, along this sight line we may be sampling different material, depending on the mixing efficiency over these length scales (Tenorio-Tagle 1996). The average hydrogen density along this sight line is $\langle n_H \rangle \equiv N(\text{H I})/d \approx 0.27 \text{ cm}^{-3}$, and Feige 110 is one of only two stars in the current *FUSE* deuterium sample to show molecular hydrogen absorption (the other being BD+28 $^\circ$ 4211; see Sonneborn et al. 2001).

Feige 110 was discovered by Feige (1958) in a search for underluminous hot stars brighter than 14 mag. In their study on the nature of faint blue stars, Greenstein & Sargent (1974) analyzed the optical spectrum of Feige 110 and obtained a rough estimate of its atmospheric parameters. Heber et al. (1984) improved Greenstein and Sargent’s analysis by using NLTE model atmospheres and determined $T_{\text{eff}} = 40,000$ K, $\log g = 5.0$, and $\log(\text{He}/\text{H}) = -1.5$. Based on the detection of strong Balmer lines, weak He I $\lambda 4471$ and He II $\lambda 4685$ lines, Heber et al. classified Feige 110 as a subdwarf OB star (sdOB). The atmospheric parameters of Feige 110 put it at the hot end of the sdB/sdOB population, which includes He-burning stars having masses close to $0.5 M_\odot$ with very thin H-rich envelopes ($M_{\text{env}} < 0.05 M_\odot$) (see, e.g., Caloi 1989; Dorman, Rood, & O’Connell 1993).

The parallax distance of Feige 110, 179 pc, is a factor of ~ 5 smaller than the distance computed using the atmospheric parameters obtained by Heber et al. (1984). This discrepancy prompted us to reanalyze the optical spectrum of Feige 110. We used three optical spectra: 1) a *STIS* spectrum retrieved from the Multimission Archive at the Space Telescope Science Institute (MAST); 2) observations taken by one of us (R.L.) at Cerro Tololo Inter-American Observatory with the 4 m telescope; and 3) observations obtained by R. Saffer (private communication) at Kitt Peak National Observatory’s 2.1 m telescope.

We estimated the atmospheric parameters of Feige 110 by comparing its optical spectrum to a grid of synthetic NLTE stellar model atmosphere spectra. We used the programs TLUSTY/SYNSPEC (Hubeny & Lanz 1995) to compute models having a pure H and He composition. The grid covered the temperature range $35,000\text{K} \leq T_{\text{eff}} \leq 50,000\text{K}$ in steps of 5,000 K for five values of the surface gravity, $\log g = 4.5, 5.0, 5.5, 6.0, 6.5$, and for four values of the helium abundance, $\log(\text{He}/\text{H}) = -1.0, -1.5, -2.0$, and -2.5 . We obtained $T_{\text{eff}} = 42,300 \pm 1,000\text{K}$, $\log g = 5.95 \pm 0.15$, and $\log(\text{He}/\text{H}) = -1.95 \pm 0.15$, by using a χ^2 minimization technique to fit the observed spectra to the synthetic spectra. These parameters are the mean values obtained from the three optical spectra. The larger gravity derived here implies a lower luminosity for Feige 110 than that derived by Heber et al., and consequently a lower distance. Our computed distance ($d = 288 \pm 43\text{ pc}$), now agrees with the Hipparcos parallax distance ($d = 179_{-67}^{+265}\text{ pc}$) within the stated uncertainties.

Feige 110 displays a very complex far-ultraviolet spectrum (Figure 1). The strong Lyman series lines of H I (Ly β up to Ly10) and the He II lines ($\lambda 1084$ up to $\lambda 942$) are the dominant stellar features. We identified all the ISM lines superimposed on the stellar spectrum of Feige 110, but were unable to identify many remaining photospheric lines. This identification is complicated by the lack of reliable atomic data, especially for the iron-peak elements. The strongest photospheric metal lines are the N IV $\lambda 923$ sextuplet, S VI $\lambda\lambda 933$ and 944 doublet, N V $\lambda 955$, N III $\lambda 979.9$ quadruplet, N III $\lambda\lambda 989.80, 991.51$, and 991.58 triplet, and P V $\lambda\lambda 1118$ and 1128 doublet. We identified photospheric lines from N, S, Cr, Fe, and Ni. Neither carbon (C III $\lambda 1175$) nor silicon (Si IV $\lambda\lambda 1122.49, 1128.33$, and 1128.49) was detected in the *FUSE* spectrum. This confirms the study of Heber et al. (1984) who reported the non-detection of carbon and silicon in the *IUE* spectrum of Feige 110.

Figure 2 shows a comparison between the synthetic spectrum and a portion of the *FUSE* spectrum. The synthetic spectrum is computed using the atmospheric parameters listed in Table 2. All the elements from H to Zn are included with solar abundances, except for He (see Table 2), C ($\sim 4 \times 10^{-6}$ solar), Si ($\sim 2 \times 10^{-7}$ solar), and Cr (21 solar). Figure 2 illustrates the difficulty in matching the model with the observed data, even though we use all atomic line data from the Kurucz & Bell (1995) database¹. The non-identification of stellar lines poses the problem of recognizing possible blends between the ISM and photospheric lines. Also, the placement of the continuum may be a problem in regions of the spectrum where many stellar lines are not identified. We take these uncertainties into consideration in our determination of the interstellar D I and O I column densities.

In addition to H I, D I, and O I, detected interstellar lines include H₂, N I, N II, Fe II, C III, P II, and Ar I. However, reliable determinations of the column densities of these species are difficult due to saturation and blending effects, and have not been done for this study.

¹Atomic data from CD-ROM 23, which is available at: <http://cfaku5.harvard.edu/cdroms.html>

4. $N(\text{D I})$ and $N(\text{O I})$ Toward Feige 110

Absorption line studies of the interstellar medium are best done with background sources consisting of hot stars with large $v\sin(i)$ values or few visible photospheric metal lines, both of which yield relatively smooth continua over the scale of typical ISM absorption lines. Unfortunately, Feige 110 does not fit this description. The far-ultraviolet continuum is very complex (Figure 1), primarily due to the large number of metal lines arising in the atmosphere of this sdOB star. Analysis of the D I and O I column densities was possible only with a judicious choice of lines which were not too severely blended with photospheric features. Proper continuum placement was somewhat uncertain and, in general, is the largest source of systematic errors in our measurements.

Two techniques have been used to estimate the column densities in this analysis. The first involves directly measuring the equivalent widths of absorption lines, which are fit to a single-component Gaussian curve of growth (COG) (Spitzer 1978). We are unaware of any high resolution optical or ultraviolet spectra that could reveal the presence of multiple components along this sight line. Furthermore, there is no evidence in the *FUSE* spectra of multiple components, which would in any case be difficult to detect unless they were separated in velocity by at least $\sim 10 \text{ km s}^{-1}$. We therefore made the simplifying assumption that a single interstellar cloud with a Maxwellian velocity distribution is responsible for the absorption. The estimates of the column density (N) and Doppler parameter (b) derived from the COG are likely to include systematic errors due to this assumption. For example, the derived b -value will not be a simple quadrature combination of thermal and turbulent velocity components, as it would be for a true single cloud. Instead, it will also reflect the spread in velocities of the multiple clouds that are likely to lie along a sight line of this length. Jenkins (1986) has discussed the systematic errors associated with the COG technique when there are multiple clouds of various strengths along a sight line, and has shown that if many non-saturated lines are used, and if the distribution of N and b -values in the clouds is not strongly bimodal, then the column density is likely to be underestimated by $\lesssim 15\%$.

Despite these shortcomings, the COG technique has the virtue of being unaffected in principle by convolution with the instrumental line spread function (LSF), provided that such convolution does not lead to unacceptable blending with neighboring lines. However, if there is a very broad component to the LSF, then in practice any technique may underestimate the column density of unsaturated components because an erroneous continuum placement could mask some fraction of the absorption. This is particularly important since the *FUSE* LSF has not yet been well characterized, though it is known to have both broad (~ 20 pixels) and narrow (~ 10 pixels) components and to change as a function of wavelength.

The second technique utilizes the profile fitting code `Owens.f`, developed by M. Lemoine and the French *FUSE* Science Team. This code models the observed absorption lines with Voigt profiles using a χ^2 minimization procedure with many free parameters, including the line spread function, flux zero point, gas temperature, and turbulent velocity within the cloud. The application of `Owens.f` to *FUSE* data is described in greater detail by Hebrard et al. (2001). Neither the COG nor profile fitting techniques include oscillator strength uncertainties in the error estimates.

4.1. The D I Analysis

To properly measure the D I equivalent widths the effects of the stellar H I Lyman series and He II absorption must be removed. This was done by shifting in velocity the synthetic stellar model discussed in §3 until the stellar H I damping wings matched the observed spectrum away from the cores of the interstellar

HI lines. The resulting average velocity difference was $\Delta V \equiv V_{\text{ISM}} - V_* = -11 \pm 9 \text{ km s}^{-1}$ and $-15 \pm 4 \text{ km s}^{-1}$ for the SiC1B and SiC2A spectra, respectively. This compares well with $\Delta V = -12 \text{ km s}^{-1}$ from measurements of five Si II ISM lines and two N V stellar lines in the *IUE* spectrum. Figure 3 shows the H I lines measured with *FUSE* as well as the profiles from the stellar model.

An additional correction to the D I absorption profiles was performed to remove blends with adjacent molecular hydrogen absorption lines. There are not enough unblended H₂ lines to determine column densities of all the rotational levels of H₂. However, only lines in the $J = 2, 3, 4$ rotational levels of H₂ are blended with the observed D I lines, and the column densities are small enough as to require only minor corrections. Therefore, we fit Gaussians to the observed profiles of unblended H₂ lines in the same rotational levels as those overlapping the D I transitions, and scaled by the relative λf - values to estimate the strength of the contaminating H₂ lines. The estimated H₂ absorption was then divided out of the stellar-normalized D I profile. Table 3 lists the unblended H₂ lines and the measured equivalent widths used to determine the H₂ corrections.

We measured the equivalent widths (W_λ) of the cleaned D I lines after fitting low-order Legendre polynomials to the local continuum profiles. This process allowed us to remove small residual flux discrepancies between the stellar model and the observed spectrum. Figure 4 shows the continuum-normalized D I profiles and our estimate of the H₂ contamination of the D I lines. The interstellar lines are at a heliocentric velocity⁷ of $V_\odot = -19 \text{ km s}^{-1}$, based on the *IUE* data. Each line was integrated over velocity limits that depended on blending and local fixed-pattern noise. The effects of scattered light are negligibly small for the D I COG analysis, and no correction was made. The measured equivalent widths are given in Table 4. The estimated errors from this method (described in detail by Sembach & Savage 1992) include contributions from both statistical and fixed-pattern noise in the local continuum, but do not include a contribution from systematic continuum placement errors of the type considered below.

The W_λ measurements were placed on a best-fit curve of growth, as shown in Figure 5. Lines from both the SiC1B and SiC2A spectra were used, with the exception of the Ly ϵ 937.548 Å line in SiC2A. As shown in Figure 4 this line is much stronger than expected. It is stronger than the same line in the SiC1B spectrum, a comparison which demonstrates the utility of the multi-channel design of *FUSE*, and stronger than the Ly δ 949.484 Å line, which cannot be correct. We believe the apparent strength of the line is due to a fixed-pattern effect on the detector, and this line is ignored in the remaining analysis.

The systematic error on each equivalent width measurement is dominated by uncertainties in the placement of the continuum. We estimate the systematic continuum placement uncertainties using the following procedure. First, the best estimate of W_λ for each line was determined using what we consider to be the proper continuum placement, and integrating over an appropriate velocity interval. Next, the maximum plausible W_λ was determined by placing the continuum at its maximum reasonable position in the region of the absorption line, and integrating over the largest reasonable velocity interval. Then the minimum plausible W_λ was measured using a similar procedure. The difference between these maximum and minimum values and the best value, whichever is greater, is taken to be a 2σ systematic error. Half of this value is combined in quadrature with the statistical error on the equivalent width measurement to give the total 1σ uncertainty. The column density computed using the COG analysis is $\log N(\text{D I})_{\text{COG}} = 15.45 \pm 0.06$ (2σ) and the Doppler parameter is $b = 6.79 \pm 0.79 \text{ km s}^{-1}$ (2σ).

An independent calculation of the D I column density was made using the profile code `Owens.f`. Seven

⁷The local standard of rest velocity is $V_{\text{LSR}} = V_\odot + 2.6 \text{ km s}^{-1}$.

D I lines in eleven separate spectral windows from the SiC1B and SiC2A spectra were simultaneously fit to the stellar continuum normalized profiles described above. Each line was constrained to a common value of the radial velocity, column density, and temperature. The continuum shape, zero flux level, and LSF were allowed to vary in each spectral window encompassing a D I line. The LSF was modelled as a Gaussian, with a FWHM that was in the range 8 – 13 pixels (16-25 km s⁻¹), depending on wavelength. A scattered light correction was made by adjusting the flux at the bottom of each neighboring saturated H I line to zero. To account for small errors in the wavelength calibration, wavelength shifts between spectral windows were permitted in the fit. The fits for each D I line are shown in Figure 6. Displayed for each line are the observed data, the continuum, and the fit after convolution with the instrumental LSF.

Various tests were done to investigate the magnitude of possible systematic uncertainties associated with the profile fitting procedure. These are described in detail in Hebrard et al. (2001), and include modelling the LSF with two Gaussians, fitting the continua with polynomials up to order 14, and varying the zero flux level from zero to twice the level at the base of each neighboring H I line. The results of these tests helped determine the magnitude of the D I column density error. The column density computed using the profile fitting analysis is $\log N(\text{D I})_{pf}=15.52 \pm 0.10$ (2σ).

We take the weighted mean of the results from the curve of growth and profile fitting procedures to arrive at our best estimate of the D I column density, $\log N(\text{D I})=15.47 \pm 0.06$ (2σ). To be conservative, we have not reduced the error below that determined from the COG result because the error is dominated by systematic effects and cannot be combined in the usual statistical fashion.

4.2. The O I Analysis

The O I column density is derived using only a COG analysis. Most of the O I lines are saturated or nearly so, which makes a profile fitting analysis difficult, especially when there are significant uncertainties in the LSF and velocity structure of the absorption profiles, as is the case in this study. In contrast to the D I analysis, no stellar model was removed prior to measuring the O I lines since the stellar profile is only slowly varying in the vicinity of these lines. The local continuum was fit using the same procedure described above for measuring the equivalent widths. No strong H₂ lines are blended with any of the O I lines used in the analysis, so no correction for H₂ was required. Small residual flux contributed by scattered light or a broad LSF has a larger effect on the estimated equivalent widths of the more saturated O I lines than the D I lines. Therefore, for each O I line a correction was made by measuring the flux at the bottom of a neighboring saturated H I line, the magnitude of which was typically ~2% of the local continuum flux. Including this correction had a negligible effect on the calculated column density, but slightly increased the estimated error.

The analysis was done in the same way as for the D I lines, again assuming a single-component Gaussian curve of growth. The statistical and systematic errors were calculated and combined in the same way as for D I. However, an additional error term resulting from a 2% uncertainty in the zero flux level (Sembach & Savage 1992) was combined in quadrature with this to determine the final error. Our best fit COG estimate gives $\log N(\text{OI})=16.73 \pm 0.10$ (2σ) and $b=6.58 \pm 0.38$ km s⁻¹ (2σ). The continuum normalized O I profiles are shown in Figure 7, and the measured equivalent widths are given in Table 5. The COG is displayed in Figure 5.

5. $N(\text{H I})$ Toward Feige 110

In the direction of Feige 110, the $\text{Ly}\alpha$ line provides the best constraint on the total H I column density because its radiation damping wings are very strong. $\text{Ly}\alpha$ is not accessible to *FUSE*. While the remaining Lyman series lines recorded in the *FUSE* spectrum are strongly saturated, they are not sufficiently strong to show well-developed damping wings. We have examined the range of b -value/column density combinations allowed by the higher Lyman series lines in the *FUSE* spectrum, and we find that these lines do not constrain $N(\text{H I})$ with sufficient precision to provide an interesting D/H measurement. At the time of this writing no suitable *HST* spectra of the Feige 110 $\text{Ly}\alpha$ line had been obtained. Consequently, we have used the only high-dispersion echelle observation of this star obtained with the short wavelength camera on *IUE* (exposure ID SWP15270) to estimate $N(\text{H I})$ toward Feige 110. This *IUE* mode provides a resolution of $\sim 25 \text{ km s}^{-1}$ FWHM and covers the 1150-1950 Å range.

5.1. *IUE* Data

The high-dispersion *IUE* observation was obtained on 1981 October 15 with an exposure time of 15.3 ksec. We reduced the data using the IUEDR processing (Giddings & Rees 1989). This reduction properly traces the echelle orders and corrects for scattered light. Note that both the IUESIPS and NEWSIPS reductions, which are available from the STScI MAST archive, have significant difficulties which make them less suitable for this analysis. The IUESIPS reduction was performed with the an early version of IUESIPS software, and was never reprocessed with the later, improved version. It apparently does not trace the orders properly, and therefore some of the signal is improperly excluded, giving rise to undulations in the extracted spectrum. In the NEWSIPS reduction the background subtraction is poor. In the fully saturated $\text{Ly}\alpha$ core, which should be centered on zero flux, the NEWSIPS spectrum shows a significant residual flux equal to ~ 16 – 19% of the continuum flux. Furthermore, the core is not flat; the residual flux is higher on the red side than on the blue side. The IUEDR reduction does not suffer from any of these difficulties.

5.2. Analysis Method

To measure the total interstellar H I column density, we used the method of Jenkins (1971); see also Jenkins et al. (1999) and Sonneborn et al. (2000). In brief, we constrained the H I column density using the Lorentzian wings of the $\text{Ly}\alpha$ profile, which have optical depth τ at wavelength λ given by $\tau(\lambda) = N(\text{H I})\sigma(\lambda) = 4.26 \times 10^{-20} N(\text{H I})(\lambda - \lambda_0)^{-2}$. Here λ_0 is the centroid of the interstellar H I absorption in this direction, which was determined from the N I triplet at 1200 Å. We estimated the value of $N(\text{H I})$ that provides the best fit to the $\text{Ly}\alpha$ profile by minimizing χ^2 using Powell’s method with five free parameters: (1) $N(\text{H I})$, (2)-(4) three coefficients that fit a second-order polynomial to the continuum (with a model stellar $\text{Ly}\alpha$ line superimposed, see below), and (5) a correction for the flux zero level. We then increased (or decreased) $N(\text{H I})$ while allowing the other free parameters to vary in order to set upper and lower confidence limits based on the ensuing changes in χ^2 .

In addition to the $\text{Ly}\alpha$ absorption profile due to interstellar H I, a subdwarf star like Feige 110 will have a substantial stellar $\text{Ly}\alpha$ absorption line with broad, Lorentzian wings as well. Neglect of this stellar line when setting the continuum for fitting the interstellar $\text{Ly}\alpha$ will lead to a substantial systematic overestimate of $N(\text{H I})$. We have used the stellar atmosphere models discussed in §3 to account for the stellar $\text{Ly}\alpha$ line. Figure 8 shows with a solid line the continuum-normalized stellar $\text{Ly}\alpha + \text{He}$ absorption profile predicted for

the most likely combination of T_{eff} , $\log g$, and He/H for this star. We superimposed the normalized stellar profile on a second-order polynomial to allow for possible instrumental calibration problems (see above). The offset of the stellar line centroid with respect to the interstellar lines was determined by comparing the velocities of several stellar and interstellar lines in the *FUSE* spectrum, and the uncertainty in the determined offset has a negligible impact on the derived $N(\text{H I})$. The dotted lines in Figure 8 indicate the shallowest and deepest stellar profiles derived from a grid of models covering the expected range of atmospheric parameters for Feige 110. We use these “extreme” stellar profiles to set upper and lower confidence limits on $N(\text{H I})$ in the following section. For purposes of illustration, the dashed line shows the stellar Ly α line predicted for the atmospheric parameters derived for Feige 110 by Heber et al. (1984); the impact of the stellar model revision on the derived interstellar $N(\text{H I})$ is discussed below.

5.3. $N(\text{H I})$ Results

Figure 9 shows the *IUE* spectrum of Feige 110; the same data are plotted in both panels but the upper panel shows a broader wavelength range to enable the reader to inspect the fit to continuum away from the strong Ly α absorption. Overplotted on the spectrum with dashed lines are the fits that provide 2σ upper and lower limits on the interstellar $N(\text{H I})$. The continua adopted for these 2σ limits are shown with dotted lines (the higher continuum corresponds to the upper limit). As noted above, in addition to the differing overall continuum level, the deepest model stellar Ly α line is assumed for the lower limit on $N(\text{H I})$, and the shallowest stellar Ly α model is assumed for the upper limit. From these fits we derive $\log N(\text{H I}) = 20.14^{+0.13}_{-0.20}$ (2σ).

We note that the revision of the stellar atmosphere parameters discussed in §3 has a substantial impact on the derived interstellar $N(\text{H I})$. If we use the older, Heber et al. (1984) atmospheric parameters to synthesize the stellar Ly α line, we obtain the stellar profile shown with a dashed line in Figure 8. With this stellar profile, we obtain an H I column density which is $\sim 0.05 - 0.2$ dex higher than that derived with our preferred stellar atmosphere parameters (see Table 2), where this range of values depends on the choice of continuum placement. Evidently, with this type of star, uncertainties in the stellar Ly α line can introduce significant systematic errors into interstellar $N(\text{H I})$ estimates. This also demonstrates the need for high quality optical data to tightly constrain the stellar model parameters.

There are, of course, many potential sources of error in estimating $N(\text{H I})$ based only on an *IUE* Ly α spectrum. To improve the estimate we attempted to measure $N(\text{H I})$ by fitting the Ly β and Ly γ lines in the *FUSE* data. However, several difficulties prevent these from further constraining $N(\text{H I})$. For example, the stellar model does not include all metal lines actually present in the stellar spectrum (see §3 and Fig. 2). The deviation of the model from the observed spectrum due to this line blanketing in many narrow spectral windows means that the effective continuum emerging from the star is overestimated by an unknown amount. Although this problem exists for all Ly lines, it is much less serious for Ly α because in this case the interstellar Lorentzian wings are stronger and much broader than the stellar Lorentzian profile. The opposite is true for Ly β and all higher Ly series lines. Thus, the continuum around Ly β is much more steeply sloping, and much harder to fit properly, and this is even worse around Ly γ .

Complicating the issue of proper continuum placement are the effects of extraneous interstellar lines in the vicinity of the H I and D I lines. Problematic species include O I and H₂, neither of which affect the Ly α profile.

Because of these problems the analysis of the Ly β and Ly γ lines did not allow an improved estimate

of $N(\text{H I})$ and we have relied exclusively on the *IUE* Ly α data. As discussed above, the systematic error associated with this is due primarily to unrecognized, narrow stellar lines. We have included the effects of known stellar lines in the continuum regions used to estimate σ for the χ^2 calculation, but nevertheless future higher resolution and signal-to-noise observations that will allow us to mask out the strong stellar lines might yield a different result. For this reason, it would be highly valuable to re-observe Feige 110 with the Space Telescope Imaging Spectrograph on board *HST*. Sonneborn et al. (2001) have shown, using high-resolution STIS observations of BD+28°4211, that such an observation can yield a very precise measurement of $N(\text{H I})$, even for a subdwarf like Feige 110.

6. Discussion

We have measured the column densities of D I, O I, and H I toward Feige 110, the longest sight line with the highest H I column density of those reported in the initial set of deuterium studies with *FUSE*. Our results are summarized in Table 6.

The D I column density was measured with two independent techniques, which give nearly the same result, despite being subject to a much different set of systematic errors. This agreement reflects the fact that there are many weak, unsaturated D I lines available for analysis, and shows the benefits of observing the high-order Lyman lines available with *FUSE*. The situation for O I is not as favorable, since most of the available lines are saturated or nearly so. This is the reason for the larger uncertainty associated with this column density measurement. Nevertheless, we are able to draw useful conclusions about the ratios of D I, O I, and H I.

Using our best column density estimates we find $\text{D}/\text{H} = (2.14 \pm 0.82) \times 10^{-5}(2\sigma)$. This deviates from some, but not all, values along sight lines both within the Local Bubble and beyond (Moos et al. 2001; Linsky 1998; Jenkins et al. 1999; Sonneborn et al. 2000). This suggests that the D/H ratio toward Feige 110 differs from that along other sight lines, both longer and shorter. This important conclusion is discussed more fully by Moos et al. (2001), who show that there is no evidence of variability within the local bubble, at distances less than ~ 100 pc, but there is significant variability at larger distances. This is discussed within the context of mixing of interstellar material driven by supernova explosions. For a uniform supernova explosion rate, material in the region may be well mixed over scales of ~ 100 pc. But if supernova events are episodic, such as those that are triggered in OB associations, there may be insufficient time to mix the material to achieve the uniformity observed in the current D/H studies. Other effects, such as the gas temperature, the volume density, and the magnetic field strength in the ISM, must be included in the models to accurately characterize the mixing time and length scales. The measurements discussed here and by Moos et al. may constrain these models.

Our result $\text{O}/\text{H} = (3.89 \pm 1.67) \times 10^{-4}(2\sigma)$, while not very precise, is in agreement with previous measurements of O/H. Meyer, Jura, & Cardelli (1998) found remarkable uniformity, $\text{O}/\text{H} = (3.43 \pm 0.77) \times 10^{-4}$ for 13 sight lines ranging in distance from 130 to 1500 pc, where the error is the 2σ dispersion in the measured values. (We have increased their published ratio by about 7.5% to account for a change in the O I 1356 oscillator strength recommended by Welty et al. (1999).) Moos et al. (2001) find no evidence of O/H variability in the sight lines studied with *FUSE*.

A very sensitive test of the idea that the deuterium abundance is decreasing with time due to stellar astration is the spatial distribution of the D/O ratio. The ionization potential of neutral H and D (13.598 eV) and O (13.618 eV) are nearly identical. Charge exchange reactions between H, D, and O keep the ionization

fractions coupled such that $D\ I/O\ I$ is a good approximation of D/O . We find $D/O = (5.50_{-1.33}^{+1.64}) \times 10^{-2}$. Moos et al. (2001) find no statistically significant spatial variation in this quantity, although the scatter about the mean value decreases if only the targets within the Local Bubble are considered. Furthermore, they find no evidence of anti-correlation between D/O and O/H . Although the metallicity range of these local ISM studies is small, this may indicate that some subtle nucleosynthetic processes are affecting the D/O ratio. One possibility discussed by Moos et al. is that there are stellar processes which destroy weakly bound deuterium nuclei without creating significant quantities of oxygen, and stellar winds mix this deuterium depleted material into the ISM. Additional measurements using *FUSE*, some of which probe sight lines to more distant targets and are currently under study, will shed more light on this interesting possibility.

This work is based on data obtained for the Guaranteed Time Team by the NASA-CNES-CSA *FUSE* mission operated by the Johns Hopkins University. Financial support to U. S. participants has been provided by NASA contract NAS5-32985. French participants are supported by CNES. This work has used the profile fitting procedure `Owens.f` developed by M. Lemoine and the *FUSE* French Team. We thank Rex Saffer for sharing his optical spectrum of Feige 110.

REFERENCES

- Abgrall, H., Roueff, E., Launay, F., Roncin, J.Y., & Subtil, J.L., 1993a, *A&AS*, 101, 273
Abgrall, H., Roueff, E., Launay, F., Roncin, J.Y., & Subtil, J.L., 1993b, *A&AS*, 101, 323
Bluhm, H., Marggraf, O., de Boer, K. S., Richter, P., & Heber, U. 1999, *A&A*, 352, 287.
Boesgard, A. & Steigman, G. 1985, *ARA&A*, 23, 319
Burles, S. & Tytler, D. 1998, *ApJ*, 499, 699
Caloi, V. 1989, *A&A*, 221, 27
Dorman, B., Rood, R. T., & O’Connell, R. W. 1993, *ApJ*, 419, 596
Epstein, R. I., Lattimer, J. M., & Schramm, D. N., 1976, *Nature*, 263, 198.
Feige, J. 1958, *ApJ*, 128,267
Giddings, J. R., & Rees, P. C. T., 1989, *SERC Starlink User Note* 37
Gözl, M. et al. 1998, in *Proc. IAU Colloq. 166, The Local Bubble and Beyond*, ed. D. Breitschwerdt, M. J. Freyberg, & J. Trumper (Berlin: Springer), 75
Greenstein, J. L., & Sargent, A. I. 1974, *ApJS*, 28, 157
Heber, U., Hamann, W.-R., Hunger, K., Kudritzki, R. P., Simon, K. P., & Méndez, R. H. 1984, *A&A*, 136, 331
Hébrard, G. et al. 2001, *ApJ*, submitted
Hubeny, I., & Lanz, T. 1995, *ApJ*, 439, 875
Jenkins, E. B. 1971, *ApJ*, 169, 25
Jenkins, E. B. 1986, *ApJ*, 304, 739.
Jenkins, E. B., Tripp, T. M., Woźniak, P. R., Sofia, U. J., & Sonneborn, G. 1999, *ApJ*, 520, 182
Kidder, K. M., Holberg, J. B., & Mason, P. A. 1991, *AJ*, 101, 579

- Kirkman, D., Tytler, D., Burles, S., Lubin, D., & O'Meara, J. M., 2000, *ApJ*, 529, 655
- Kruk, J.W. et al. 2001, *ApJ*, submitted
- Kurucz, R., & Bell, B. 1995, *Atomic Line Data Kurucz CD-ROM No. 23*, (Cambridge, Mass.: Smithsonian Astrophysical Observatory)
- Lallement, R. & Bertin, P. 1992, *A&A*, 266, 479
- Lehner, N. et al. 2001, *ApJ*, submitted
- Lemoine, M. et al. 2001, *ApJ*, submitted
- Linsky, J. L. et al. 1995, *ApJ*, 451, 335
- Linsky, J. L. 1998, *Space Sci. Rev.* 84, 285
- Meyer, D. M., Jura, M., & Cardelli, J. A., *ApJ*, 493, 222.
- Morton, D.C. 1991, *ApJS*, 77, 119
- Moos, H. W. et al. 2000, *ApJ*, 538, L1
- Moos, H. W. et al. 2001, *ApJ*, submitted
- Perryman, M. A. C., et al. 1997, *A&A*, 323, L49
- Reeves, H., Audouze, J., Fowler, W., & Schramm, D., N. *ApJ*, 179, 909
- Rogerson, J. B. & York, D. G. 1973, *ApJ*, 186, L95
- Sahnow, D. J. et al. 2000, *ApJ*, 538, L7
- Sahu, M. S. et al. 1999, *ApJ*, 523, L159.
- Sembach, K. R. & Savage, B. D. 1992, *ApJS*, 83, 147
- Sfeir, D. M., Lallement, R., Crifo, F., & Welsh, B. Y. 1999, *A&A*, 346, 785
- Sonneborn, G., Tripp, T. M., Ferlet, R., Jenkins, E. B., Sofia, U. J., Vidal-Madjar, A., & Woźniak, P. R. 2000, *ApJ*, 545, 277
- Sonneborn, G. et al. 2001, *ApJ*, submitted
- Spitzer, L. 1978, *Physical Processes in the Interstellar Medium* (New York: John Wiley)
- Tenorio-Tagle 1996, *AJ*, 111, 1641
- Tosi, M. et al. 1998, *ApJ*, 498, 226
- Vidal-Madjar, A. & Gry, C. 1984, *A&A*, 138, 285.
- Vidal-Madjar, A. et al. 1998, *A&A*, 338, 694.
- Welty, D.E. et al. 1999, *ApJS*, 124, 465
- Wood, B.E. et al. 2001, *ApJ*, submitted

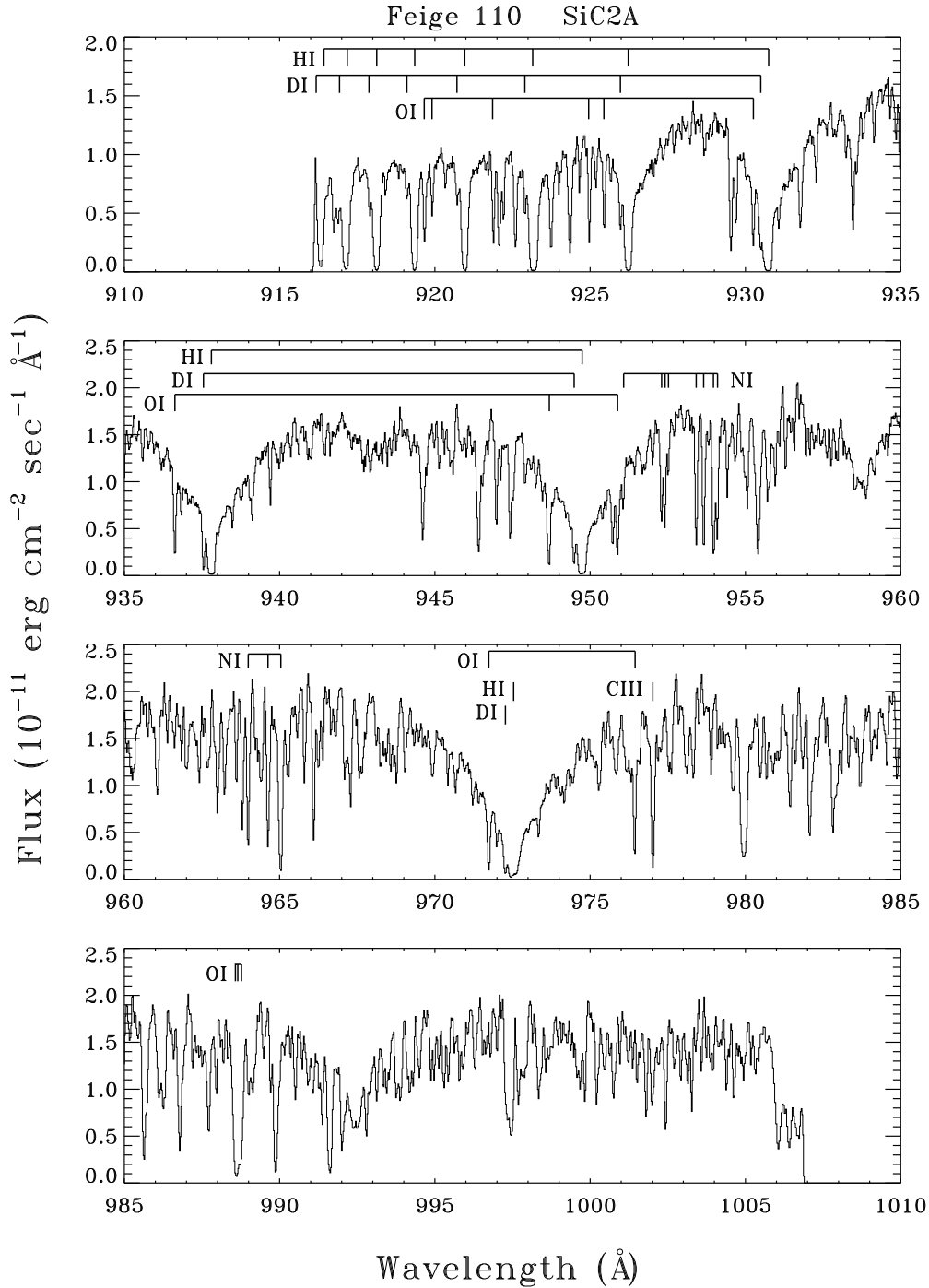


Fig. 1.— The SiC2A spectrum, showing absorption lines used in the analysis of the D I and O I column densities. Interstellar D I, H I, O I, N I, and C III lines have been marked. Many of the remaining lines are due to interstellar H₂, or metal lines arising in the atmosphere of this subdwarf OB star. The data have been binned by 4 pixels ($\sim 0.024 \text{ \AA}$) in this figure. Note the flux scale change between the panels.

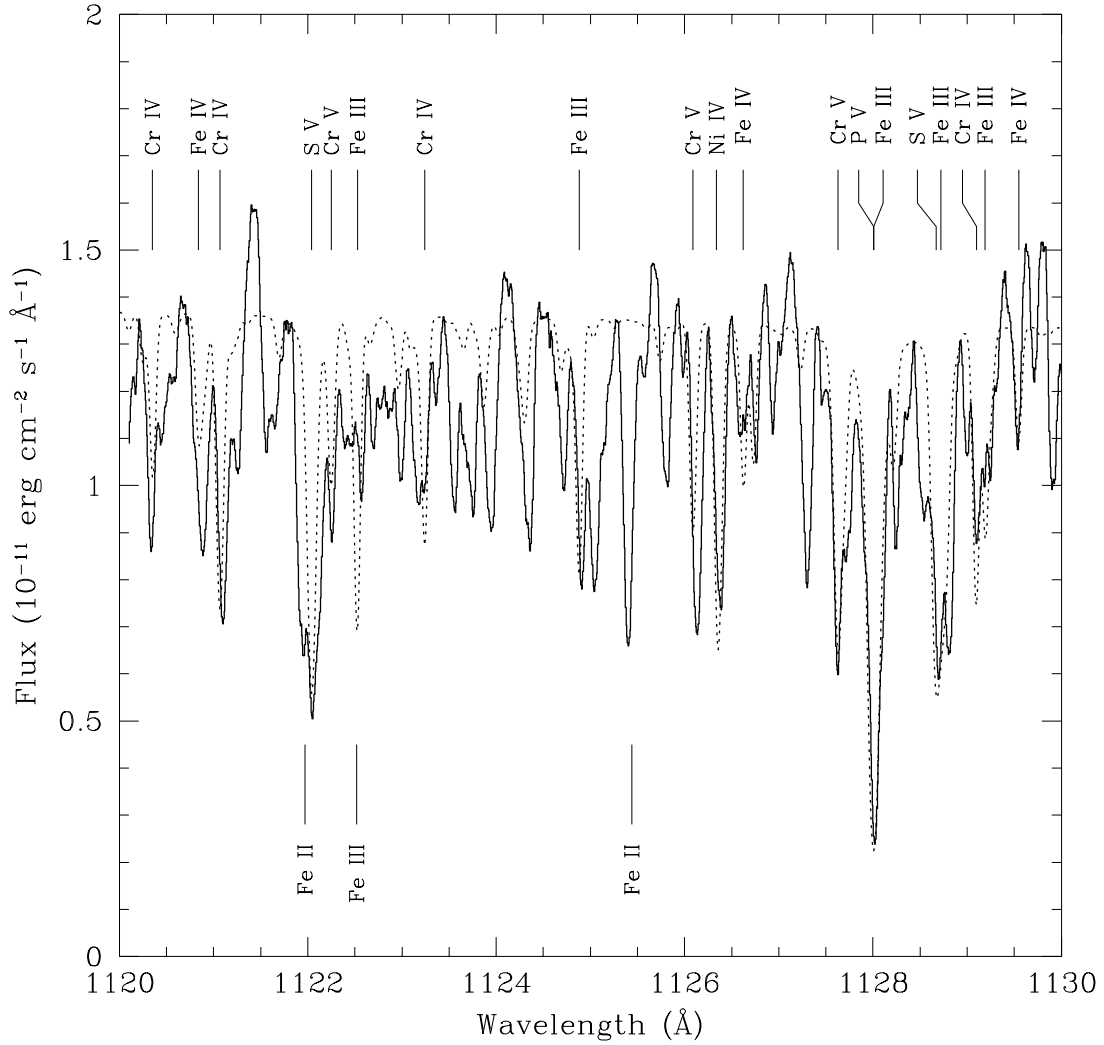


Fig. 2.— Portion of the *FUSE* spectrum (*solid line*) compared to the synthetic spectrum (*dotted line*). The identified photospheric lines are labelled above the spectrum, and the ISM lines are labelled below the spectrum. The lack of reliable atomic data for the stellar lines is apparent in this portion of the spectrum. Note the absence of any Si IV $\lambda\lambda 1122.49$, 1128.33 , and 1128.49 features in the *FUSE* spectrum, as noted in the text.

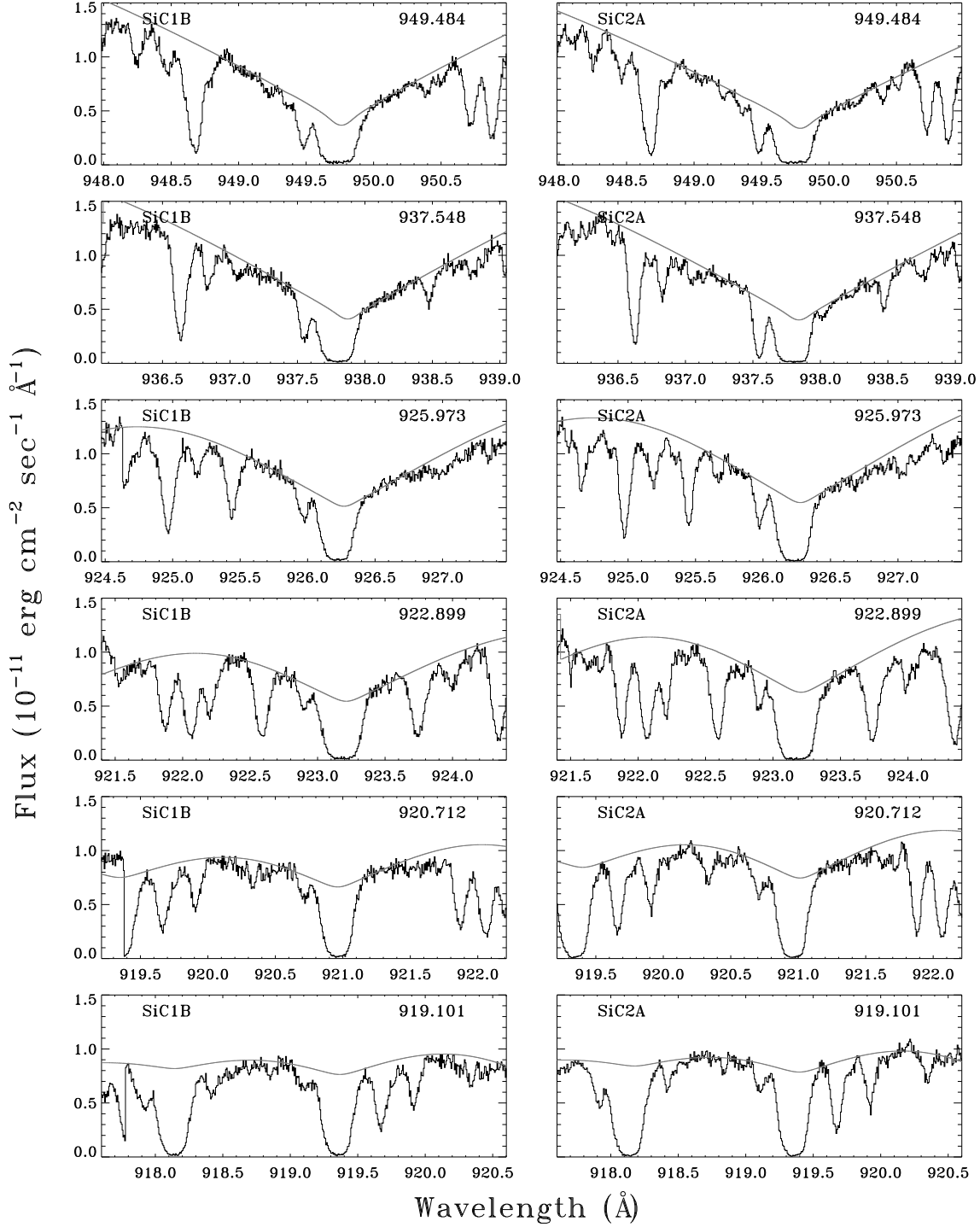


Fig. 3.— The absorption line profiles used in the analysis of the D I column density. The thin line in each panel shows the stellar model, which has been shifted in wavelength and scaled in flux to match the continuum away from the core of the interstellar H I absorption. The spectra from segment SiC1B are in the left panels, and those from segment SiC2A are in the right panels.

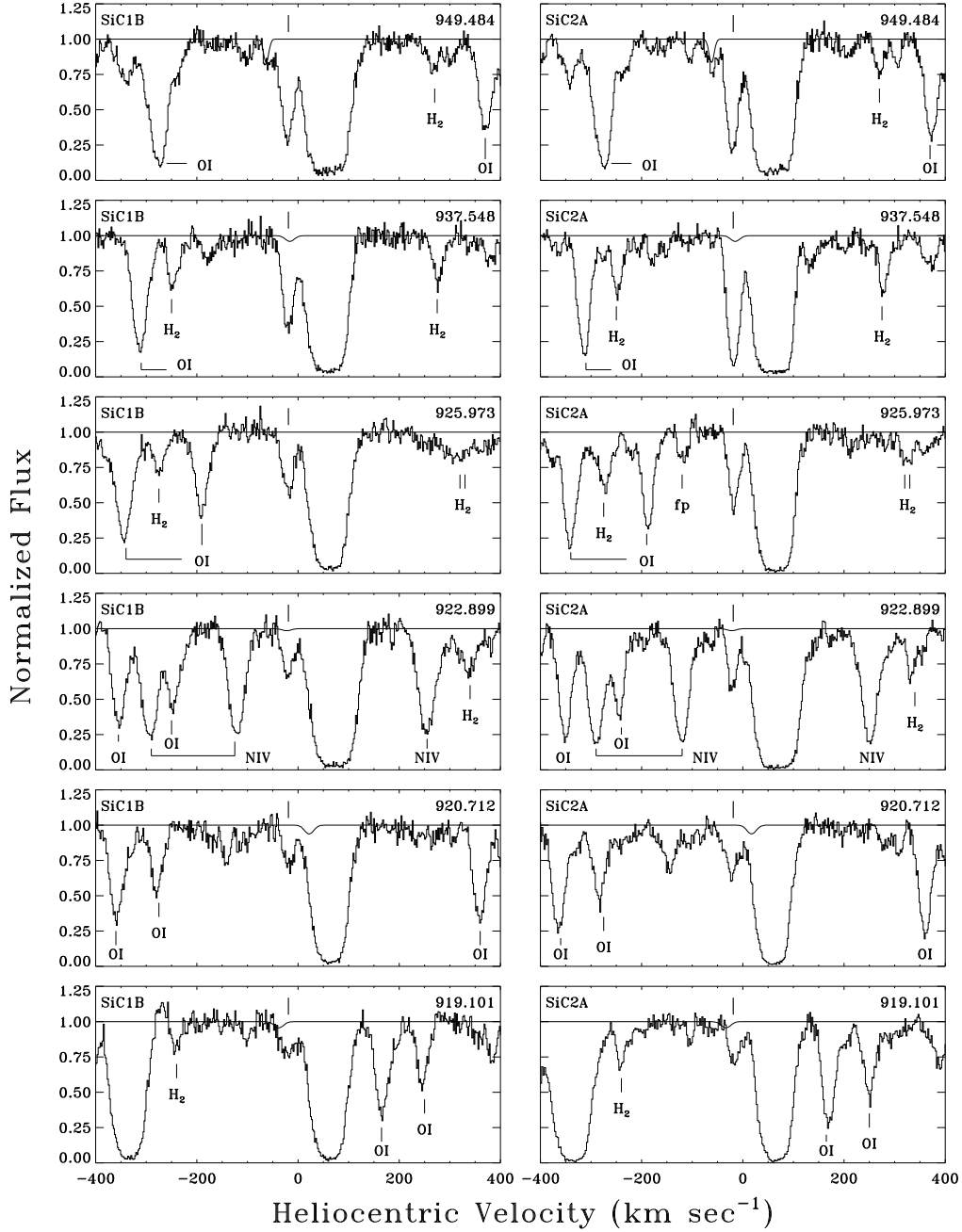


Fig. 4.— Continuum normalized D I absorption profiles, which are centered at a velocity $V_{helio} = -19$ km s^{-1} . The positions of the D I lines are indicated by vertical tick marks above the spectra. Superimposed on the smooth continuum line of each profile is the Gaussian H_2 line whose equivalent width and FWHM have been calculated based on unblended H_2 lines in the same rotational level, which are listed in Table 3. (The D I $\lambda 925.973$ line is not blended with H_2 .) The $\lambda 937.548$ line in the SiC2A spectrum is much stronger than expected, and is probably contaminated by a detector defect. It has not been included in the D I analysis. A detector fixed-pattern feature is denoted by "fp." The spectra from segment SiC1B are in the left panels, and those from segment SiC2A are in the right panels.

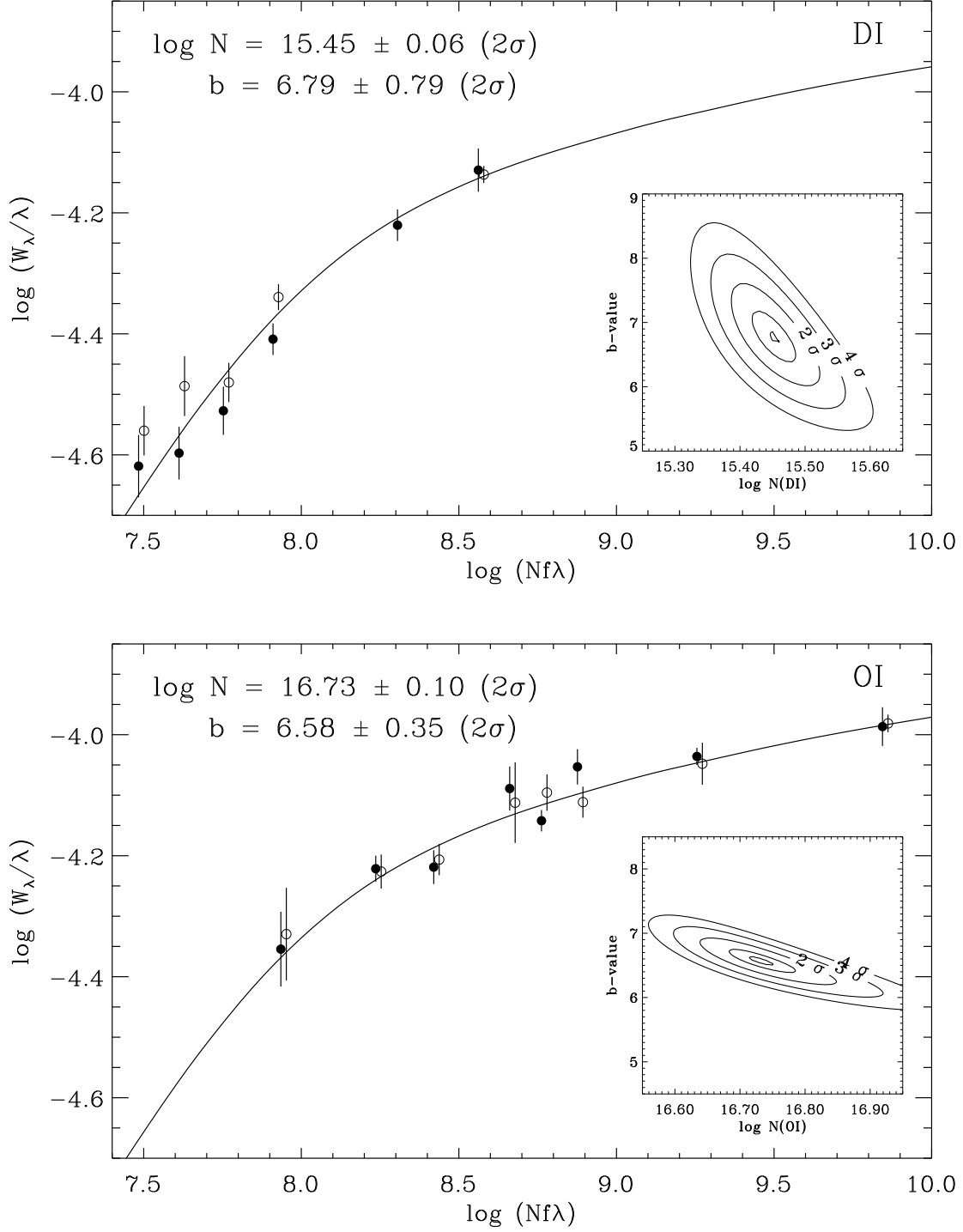


Fig. 5.— The curves of growth for D I (top) and O I (bottom). In both cases, a single-component, Gaussian curve of growth has been assumed. The insets show the $\log(N)/b$ -value error contours. The large number of weak D I lines available tightly constrain the D I column density. Most of the O I lines are partially or fully saturated, so the column density is less well constrained. For clarity, at each wavelength the data points derived from the SiC1B spectra (solid circles) and the SiC2A spectra (open circles) have been slightly separated horizontally.

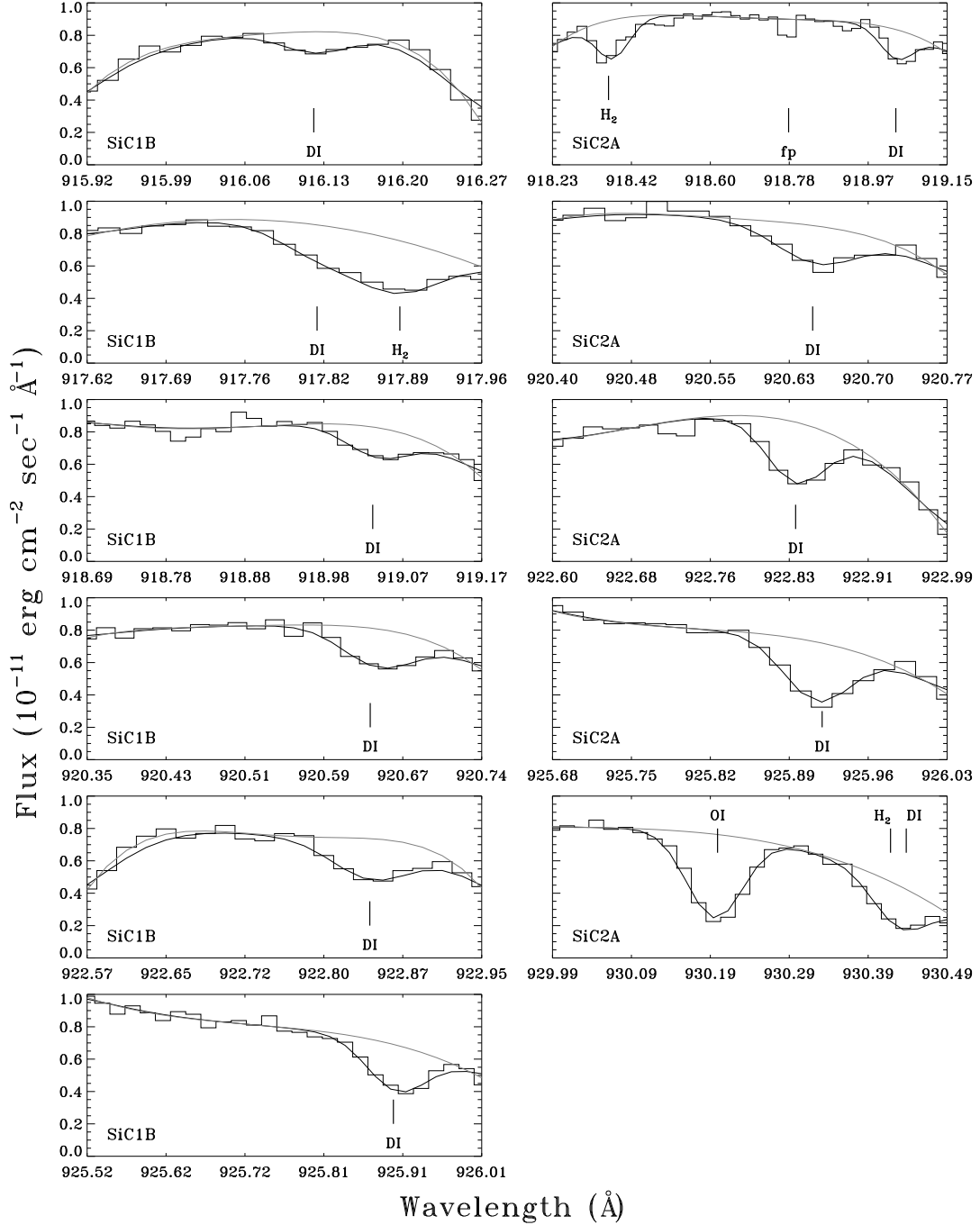


Fig. 6.— Fits to the D I lines using the `Owens.f` profile fitting code. The histogram line is the observed spectrum and the thin black line is the computed fit. The light gray line shows the continuum. A detector fixed-pattern feature is denoted by "fp." The spectra from segment SiC1B are in the left panels, and those from segment SiC2A are in the right panels.

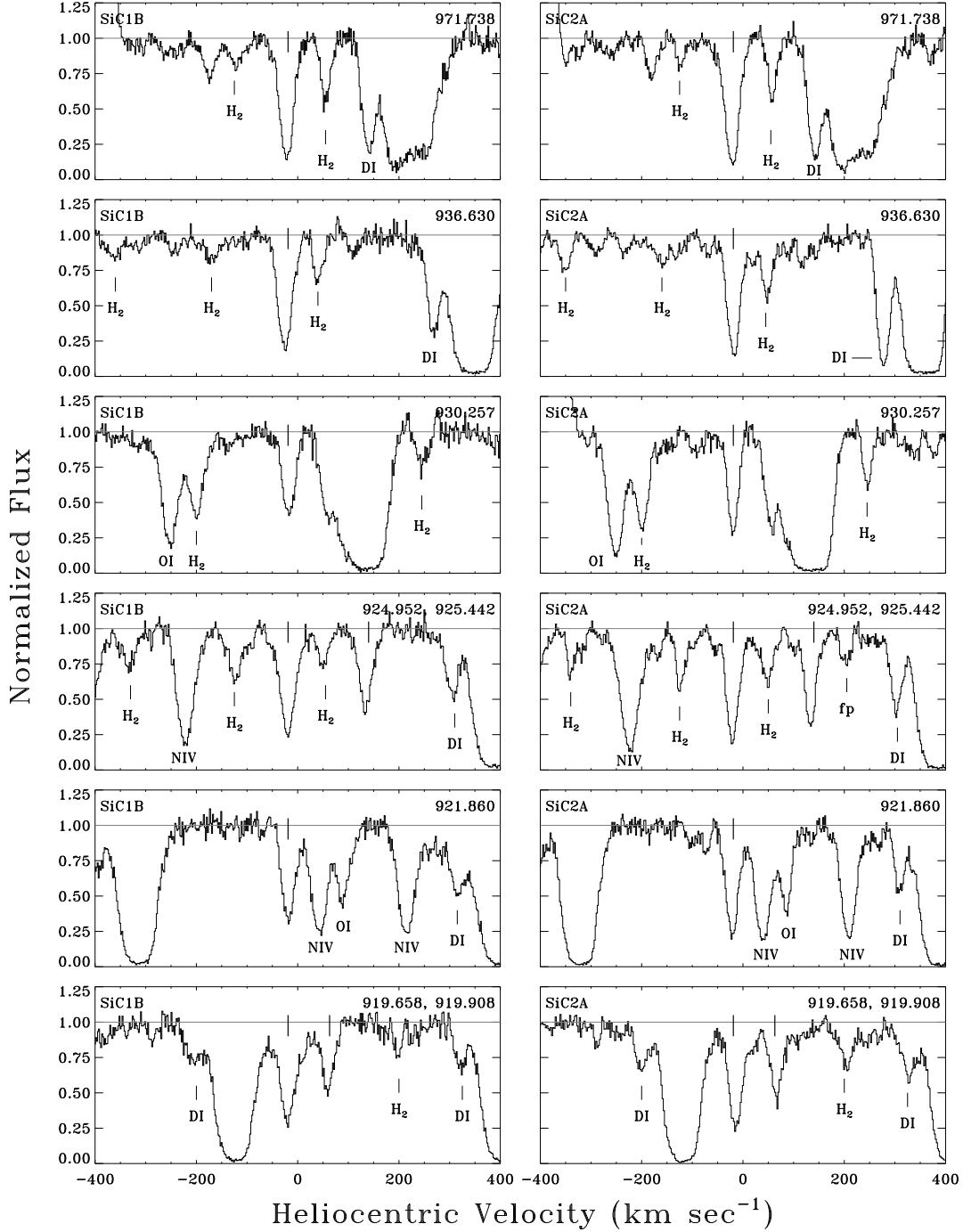


Fig. 7.— Continuum normalized O I absorption profiles. The positions of the O I lines used in the column density analysis are indicated by the vertical tick marks above the spectra. These are the only O I lines for which a continuum level could be established with reasonable confidence. The spectra from segment SiC1B are in the left panels, and those from segment SiC2A are in the right panels.

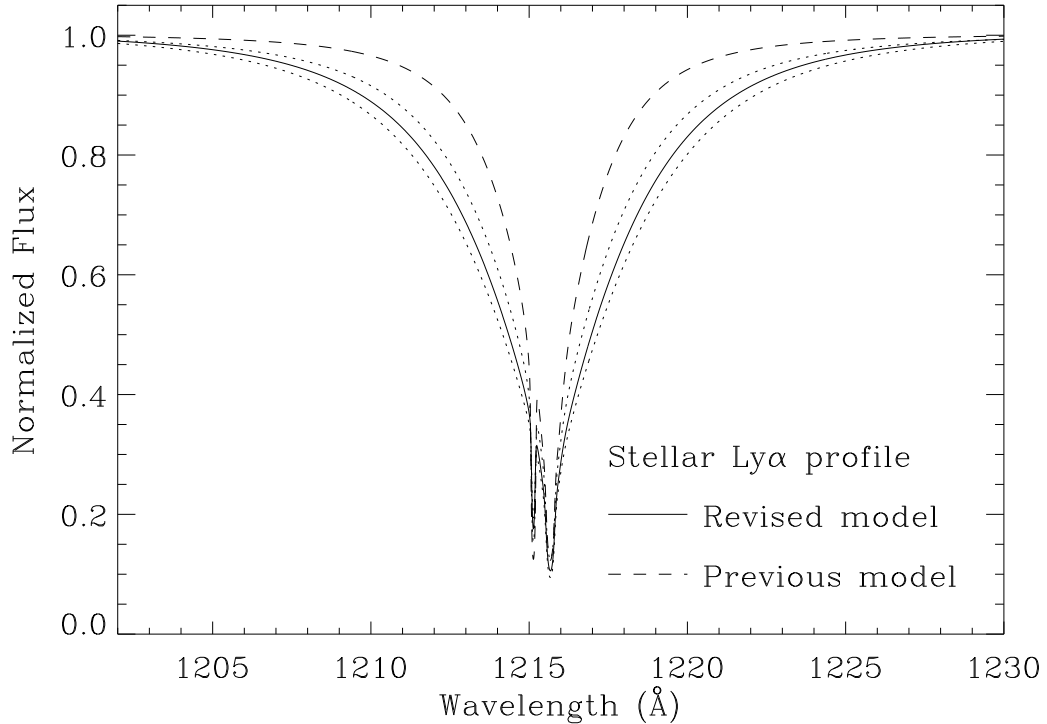


Fig. 8.— Synthetic stellar spectra of Feige 110 in the vicinity of the stellar Ly α line, normalized to the adjacent continuum. The Ly α profile resulting from our preferred parameters for the stellar atmosphere (see §3) is plotted with a solid line, and the dotted lines show the highest and lowest profiles found in a grid of 27 models spanning the expected range of T_{eff} , $\log g$, and He/H for this star. The revision of the stellar model has a significant impact on the stellar Ly α profile. To show this, the dashed line indicates the profile which would result from the previously published analysis (see §3).

Table 1. Feige 110 Observation Log

Instrument	Date	Program ID	Exposures	Exposure Time
<i>FUSE</i>	22 June 2000	M1080801	001 - 008	6228
<i>FUSE</i>	30 June 2000	P1044301	019 - 066 ^a	21779
<i>IUE</i>	15 October 1981	...	SWP 15270	15300

^aExposures 001-018 missing due to an acquisition problem with the previous observation.

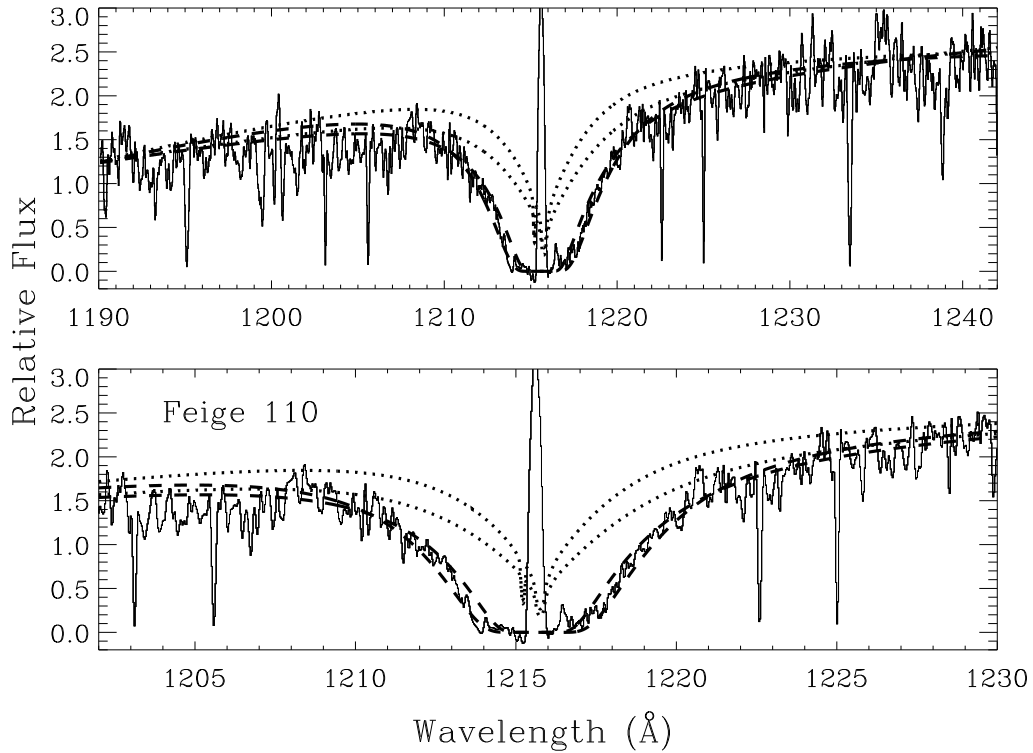


Fig. 9.— High-dispersion *IUE* observation of Feige 110 (histogram) with the fitted profiles (dashed lines) for the upper and lower bounds on $N(\text{H I})$ at the 2σ confidence level. The continua corresponding to the upper and lower bounds are shown with dotted lines; the upper bound uses the higher continuum placement. The upper and lower panels plot the same data and fits on different scales to enable the reader to inspect the details in the Ly α profile as well as the continuum fit well away from the interstellar H I line. The large, narrow spikes which dip down to nearly zero flux are artifacts due to the joining of echelle orders in the *IUE* spectrum or reseau marks on the face plate of the *IUE* camera.

Table 2. Target and Sight Line Parameters for Feige 110

Quantity	Value	Reference
Spectral Type	sdOB	1
(l, b)	$(74^\circ 09, -59^\circ 07)$	2
d^a (pc)	179^{+265}_{-67}	2
z (pc)	-154^{+57}_{-227}	2
V	11.86	3
$U - B$	-1.19	3
$B - V$	-0.33	3
T_{eff} (K)	42300 ± 1000	4
$\log g$ (cm s^{-2})	5.95 ± 0.15	4
$\log(\text{He}/\text{H})$	-1.95 ± 0.15	4
$\log N(\text{H I})$	$20.18^{+0.14}_{-0.21}$	4
$\langle n_H \rangle$	0.27 cm^{-3}	4

^aDerived from trigonometric parallax

References. — (1) Heber et al. 1984; (2) Perryman et al. 1997; (3) Kidder et al. 1991; (4) this study.

Table 3. H₂ Equivalent Widths

Line Identification	$\lambda(\text{\AA})$	$\log \lambda f^a$	$W_\lambda \text{ [m\AA]}^b$			
			SiC1B	SiC2A	LiF1A	LiF2B
W (3-0) R(2)	947.111	1.101	12.6 ± 3.4	10.4 ± 1.2
W (3-0) Q(3)	950.397	1.417	14.2 ± 2.8	14.4 ± 1.9
W (2-0) Q(4)	971.387	1.533	16.2 ± 3.6	12.0 ± 2.1
L (6-0) P(3)	1031.191	1.059	48.7 ± 4.1	45.6 ± 2.3

^aOscillator strengths from Abgrall et al. 1993a,b.

^bMeasured equivalent widths and 1σ uncertainties (in mÅ).

Table 4. D I Equivalent Widths

$\lambda(\text{\AA})$	$\log \lambda f^{\text{a}}$	$W_{\lambda} [\text{m\AA}]^{\text{b}}$	
		SiC1B	SiC2A
919.101	0.0425	22.1 ± 2.8	25.3 ± 2.5
920.712	0.171	23.3 ± 2.5	30.0 ± 3.6
922.899	0.312	27.4 ± 2.6	30.5 ± 2.4
925.973	0.469	36.1 ± 2.2	42.4 ± 2.2
937.548	0.864	56.4 ± 3.5	...
949.484	1.121	70.5 ± 6.1	69.3 ± 2.3

^aOscillator strengths from Morton 1991.

^bMeasured equivalent widths and 1σ uncertainties (in mÅ).

Table 5. O I Equivalent Widths

$\lambda(\text{\AA})$	$\log \lambda f^{\text{a}}$	$W_{\lambda} [\text{m\AA}]^{\text{b}}$	
		SiC1B	SiC2A
919.658	-0.060	74.9 ± 6.5	71.0 ± 11.8
919.917	-0.786	40.7 ± 6.2	43.1 ± 8.3
921.857	0.041	66.4 ± 2.8	74.0 ± 5.3
924.950	0.155	81.9 ± 5.7	71.6 ± 4.4
925.442	-0.485	55.6 ± 2.8	55.0 ± 3.7
930.257	-0.301	56.2 ± 3.7	57.8 ± 3.5
936.630	0.534	86.2 ± 2.9	83.9 ± 7.0
971.738	1.123	100.2 ± 7.7	101.4 ± 3.5

^aOscillator strengths from Morton 1991 and Morton (private communication).

^bMeasured equivalent widths and 1σ uncertainties (in mÅ).

Table 6. Summary of Results of This Study

Quantity	Value (2σ errors)
$\log N(\text{D I})$	15.47 ± 0.06
$\log N(\text{O I})$	16.73 ± 0.10
$\log N(\text{H I})$	$20.14^{+0.13}_{-0.20}$
D/H	$(2.14 \pm 0.82) \times 10^{-5}$
O/H	$(3.89 \pm 1.67) \times 10^{-4}$
D/O	$(5.50^{+1.64}_{-1.33}) \times 10^{-2}$